THE JOURNAL OF PHYSICAL CHEMISTRY C

Article

pubs.acs.org/JPCC

# Direct Synthesis of Vanadium Phthalocyanine and Its Electronic and Magnetic States in Monolayers and Multilayers on Ag(111)

Keitaro Eguchi,[†] Takeshi Nakagawa,[†,‡] Yasumasa Takagi,[†,‡] and Toshihiko Yokoyama*[,†,‡]

[†]Department of Structural Molecular Science, SOKENDAI, The Graduate University for Advanced Studies, Myodaiji, Okazaki 444-8585, Japan

[‡]Department of Materials Molecular Science, Institute for Molecular Science, Myodaiji, Okazaki 444-8585, Japan

Supporting Information

**ABSTRACT:** Vanadium phthalocyanine (VPc) monolayers and multilayers were synthesized on Ag(111), and the electronic and magnetic states of an unachieved VPc with a divalent state of V were investigated. The VPc monolayer was fabricated by directly depositing the V atoms on a metal-free phthalocyanine ($H_2Pc$) monolayer under ultrahigh-vacuum conditions. The VPc multilayer was synthesized by repeated VPc monolayer deposition and subsequent sample annealing at approximately 450 K. The N 1s X-ray photoelectron spectra (XPS) of these samples showed a remarkable reduction in the peak assigned to H-bonded N atoms, concomitant with the appearance of a new peak attributed to V-bonded N atoms close to the peak of iminic N. Additionally, the oxidation state of V estimated from the V 2p XPS peak position corresponded to 1.6 and 2.4 in the monolayer and multilayer samples, respectively. These results clearly imply that VPc monolayers and multilayers were successfully obtained. The main ground-state electronic configuration of the V center was found to be $^2E_g$ by angle-dependent V L-edge X-ray absorption spectroscopy. Furthermore, X-ray magnetic circular dichroism (XMCD) measurements suggest that this $^2E_g$ state was mixed with the $^2A_{1g}$ state by spin−orbit coupling in the ground state. Data revealed that VPc shows a paramagnetic state on the Ag surface and in an $H_2Pc$ film but an antiferromagnetic state in the multilayer. Partial electron charge transfer was also observed from the Ag surface to the V center at the VPc/Ag(111) interface, leading to a significant decrease in XMCD signals in the monolayer.

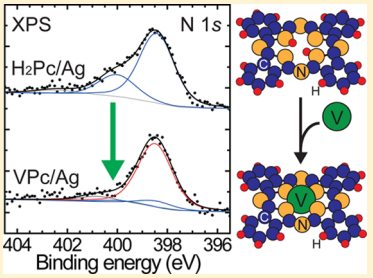


## 1. INTRODUCTION

Superior and unique characteristics, such as relatively high thermal and chemical stabilities as well as optical and semiconducting properties, have contributed to the wide use of metal phthalocyanines (MPcs) in industrial products like dyes,[1] gas sensors,[2] organic light-emitting diodes,[3] and organic photovoltaics.[4] While these properties have attracted interest in organic and molecular electronics,[5] the recent discovery of exciting magnetic properties in MPcs has extended their application to molecular spintronics.[6,7] To functionalize and manipulate intentionally their electronic and magnetic states in organic films and/or on substrate surfaces, it is important to systematically understand these properties of MPcs.

Typically, MPcs consist of a central metal ion and a $\pi$-conjugated macrocycle. Since the discoveries of CuPc and FePc in 1927 and 1928, respectively,[1] several types of MPcs have been synthesized by changing central metal ions and coordination atoms and/or modifying the phthalocyanine ligand. In the 3d transition metal series, all metal ions could be coordinated to the phthalocyanine ligand. However, the synthesis of MPcs in which the central metal ion presents a simple divalent state has been limited to Ti, Cr, Mn, Fe, Co, Ni, Cu, and Zn.[8] Although Sc and V have displayed trivalent and/or quadrivalent states in scandium diphthalocyanine ($ScPc_2$),[9] iodo(phthalocyaninato)vanadium(III) (VIPc),[10] and oxyvanadium phthalocyanine (VOPc),[11] ScPc and VPc comprising a divalent metal center have not been synthesized to date because of their instability in air. The absence of these molecules limits our understanding of MPc electronic and magnetic structures, making their synthesis necessary. This study focused on VPc as a target compound because chemically stable VOPc is easily obtained by a chemical method and its electronic and magnetic properties have been investigated in bulk,[12] thin films,[13] and monolayers.[14,15]

One way to generate VPc is direct synthesis on a substrate in the absence of air, as reported by Gottfried et al.[16] In this previous report, Co-tetraphenylporphyrin (CoTPP) was obtained by vapor deposition of tetraphenylporphyrin ($H_2TPP$) molecules and Co atoms on Ag(111) under ultrahigh vacuum (UHV) conditions. This approach has also proven useful for MPc and metal porphyrin (MPor) synthesis, particularly FeTPP,[17−21] CoTPP,[21,22] NiTPP,[23,24] ZnTPP,[22,25,26] CeTPP,[27,28] iron tetramethylporphyrin,[29] and FePc,[30] which have been characterized by X-ray photoelectron spectroscopy (XPS) and scanning tunneling microscopy (STM). The chemical reaction involved in this direct synthesis has also been studied in detail by theoretical calculations and thermal desorption spectroscopy (TDS).[22,26] Gas-phase

**Received:** December 28, 2014
**Revised:** April 15, 2015
**Published:** April 16, 2015

ACS Publications © 2015 American Chemical Society



DOI: 10.1021/jp512935v
J. Phys. Chem. C 2015, 119, 9805−9815

theoretical calculations of an unsubstituted porphyrin have provided a three-step mechanism for this reaction. Briefly, the metal atom is first captured by four central N atoms, and one H atom bound to a pyrrolic N atom is subsequently transferred to this central metal. Finally, the other H atom is also transferred to the metal and $H_2$ molecule desorption produces MPor.[22,26] As expected from the theoretical calculations, $D_2$ desorption from $D_2$TPP was confirmed by TDS.[26] In addition, these previous reports showed that the reactivity depends on the nature of the central metal and the activation barrier decreases in the order Zn, Cu, Ni, Co, and Fe.[26] Therefore, this well-established method may be suitable for the synthesis of air-unstable metal complexes.

The electronic and magnetic properties of MPcs, particularly those containing 3d metal centers, have been investigated experimentally and theoretically. In typical planar MPcs, the 3d orbital of the metal ion is split into $a_{1g}$ ($d_{z^2}$), $b_{1g}$ ($d_{x^2-y^2}$), $b_{2g}$ ($d_{xy}$), and $e_g$ ($d_{xz}$, $d_{yz}$) levels because of the $D_{4h}$ symmetrical molecular structure. Although these MPcs presented various unique properties, the $b_{1g}$ orbital exhibited the highest energy level irrespective of the central metal ion,[31,32] while the other three orbitals were considered close to each other, making the electronic state difficult to determine. Theoretical calculations suggested that the 3d electrons displayed the configurations $a_{1g}^2 b_{2g}^2 e_g^4 b_{1g}^2$ in ZnPc, $a_{1g}^2 b_{2g}^2 e_g^4 b_{1g}^1$ in CuPc, and $a_{1g}^2 b_{2g}^2 e_g^4 b_{1g}^0$ in NiPc.[31,32] These electronic configurations have been validated by X-ray absorption spectroscopy (XAS).[33,34] They suggest the existence of spin in CuPc but no spin in ZnPc and NiPc, which is in good agreement with electron paramagnetic resonance (EPR)[35] and magnetic susceptibility[36,37] measurements.

The electronic configuration of the central metal ion becomes more complicated when the number of 3d electrons is less than seven. Theoretical calculations have indicated that the ground state of Co corresponded to $^2A_{1g}$ ($b_{2g}^2 e_g^4 a_{1g}^1 b_{1g}^0$)[31,38,39] and $^2E_g$ ($b_{2g}^2 a_{1g}^2 e_g^3 b_{1g}^0$)[32] in CoPc. Angle-dependent XAS[33] and magnetic susceptibility[40] measurements have suggested the $^2A_{1g}$ state as the ground state. A mixed state of $^2A_{1g}$ and $^2E_g$ has also been proposed to explain the large effective magnetic moments of CoPc obtained by magnetic susceptibility measurements.[41] CoPc has exhibited paramagnetic behavior in its $\alpha$ and $\beta$ phases above 80 K. Further, Serri et al.[42] have observed high-temperature (~100 K) antiferromagnetic coupling in an $\alpha$-CoPc thin film.

Similarly, several electronic configurations have been suggested for FePc and MnPc. Theoretical calculations have predicted $^3E_gA$ ($b_{2g}^2 e_g^3 a_{1g}^1 b_{1g}^0$)[31] and $^3A_{2g}$ ($b_{2g}^2 a_{1g}^2 e_g^2 b_{1g}^0$)[32,43] as ground states for FePc. The $^3E_gA$ ground state in $\alpha$- and $\beta$-FePc has been widely supported by magnetic susceptibility,[44] Mössbauer,[45] XAS,[33,46] and X-ray magnetic circular dichroism (XMCD)[47] measurements, whereas few experimental results have observed the $^3A_{2g}$ state.[48] In addition to these states, a potential $^3B_{2g}$ ground state ($e_g^4 b_{2g}^1 a_{1g}^1 b_{1g}^0$)[49] and a spin-mixed state of the triplet and quintet states[50] have been proposed by magnetic susceptibility and a combined experimental XAS–theoretical approach, respectively. Magnetic properties of FePc strongly depend on its crystal structure. In the most stable $\beta$-FePc phase, magnetic interactions between FePc molecules were moderate and Weiss temperatures of −9 K[41] and 7 K[51] were reported. On the other hand, Evangelisti et al.[44] have observed ferromagnetic behavior in $\alpha$-FePc at a Curie temperature of approximately 10 K. This ferromagnetic behavior has also been detected in FePc thin films fabricated on sapphire, Si, and Au substrates.[52,53] In addition, large $g$-values of 2.4–2.6 have been reported in $\alpha$- and $\beta$-FePc,[41,44] suggesting a large contribution of an unquenched orbital magnetic moment. Magnetic susceptibility measurements of MnPc single crystals[41,54−56] and theoretical calculations[31] have indicated that the $^4A_{2g}$ ($b_{2g}^2 e_g^2 a_{1g}^1 b_{1g}^0$) state is a ground state for MnPc. In addition, XAS[57] and XMCD[58] of MnPc thin films, UV–visible MCD spectra of MnPc in Ar gas,[59] and theoretical calculations[60,61] have proposed the $^4E_g$ ($b_{2g}^1 e_g^3 a_{1g}^1 b_{1g}^0$) state as a ground state. In contrast to FePc, MnPc has presented a ferromagnetic state in the $\beta$ phase below 8.3–8.6 K.[55,56,58] The $\alpha$-MnPc phase showed a Weiss temperature of −3 K in magnetic susceptibility measurements.[62]

The effective magnetic moment of CrPc was estimated as 3.49$\mu_B$ at room temperature, which lay between high ($S$ = 2) and intermediate ($S$ = 1) spin states.[41] However, the details of its electronic and magnetic properties remain unclear. The electronic and magnetic properties of TiPc are also unsolved, although its synthesis has been reported.[8] To the best of our knowledge, no experimental or theoretical study has been reported for VPc or ScPc. The occupancy of 3d orbitals in less than half the 3d electron systems, the order of the split 3d orbitals, and their spin multiplet and magnetic states also remain ill-understood, making the electronic and magnetic states of VPc worth investigating.

In this study, VPc monolayers and multilayers were synthesized by depositing V atoms and metal-free phthalocyanine ($H_2$Pc, Figure 1a) on Ag(111) under UHV conditions.

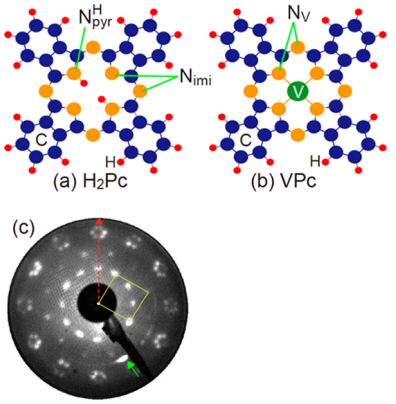


**Figure 1.** Molecular structures of (a) $H_2$Pc and (b) VPc. Each N atom appears as $N_{imi}$ (−N=) and $N^H_{pyr}$ (−NH−) for $H_2$Pc and $N_V$ for VPc. (c) Low-energy electron diffraction (LEED) pattern of the $H_2$Pc monolayer on Ag(111) obtained at an incident electron energy of 11 eV. Yellow lines represent the $H_2$Pc lattice. The red arrow shows the direction of Ag [11$\bar{2}$]. The green arrow marks a sham spot originating from the filament's artificial light.

The metalation reaction was evaluated by in situ XPS. Subsequently, the electronic and magnetic states of VPc were investigated by XAS and XMCD. This is the first report on synthesis of VPc and characterization of its electronic and magnetic states.

## 2. EXPERIMENTAL SECTION

Sample preparation was performed under UHV conditions (base pressure of ~2 × $10^{-8}$ Pa). The VPc monolayer was synthesized in the XPS chamber as follows. Clean Ag(111) was obtained by repeating a cycle of Ar ion sputtering and annealing at 800 K. Its ordering structure and cleanliness were checked by


DOI: 10.1021/jp512935v
J. Phys. Chem. C 2015, 119, 9805–9815

low-energy electron diffraction (LEED) and Auger electron spectroscopy (AES). No contamination of Ag(111) with a sharp (1 × 1) LEED pattern was detected. Commercial $H_2Pc$ (purity >98%) was purified by sublimation and introduced in a homemade Knudsen cell equipped with an alumel−chromel (K-type) thermocouple. An $H_2Pc$ monolayer was formed on Ag(111) at room temperature (RT) by using the Knudsen cell. The deposition rate of $H_2Pc$ was set at approximately 0.1 monolayer (ML)/min by adjusting the cell temperature to 470 K. The molecular density of the $H_2Pc$ monolayer was defined as 0.5 molecule/nm$^2$, and the $H_2Pc$ monolayer self-assembly was assessed by LEED (Figure 1c). The obtained LEED pattern was almost the same as in previous reports.[63,64] Next, a stoichiometric amount of V (0.5 atom/nm$^2$) was deposited on the $H_2Pc$ film by electron bombardment evaporation. The deposited amount of V was estimated by use of the monitor of a quartz crystal oscillator and by comparing the V 2p XPS intensity with that of the VOPc monolayer on Ag(111).[14] The LEED pattern showed no significant change after the deposition of V. The VPc multilayer (10 ML) was obtained by repeating the cycle of deposition of $H_2Pc$ and V 10 times and was subsequently annealed at approximately 450 K for 15 min.

XPS measurements were performed at 300 K in a UHV chamber ($P < 4 \times 10^{-8}$ Pa). The sample was irradiated with a non-monochromatized Mg K$\alpha$ beam ($h\nu$ = 1253.6 eV) at an incidence angle of 45° with respect to the surface normal. Photoelectron signals were detected by a hemispherical electron analyzer (SPECS, Phoibos 100) that faced the sample surface (normal emission detection). Binding energies were calibrated by use of the Ag $3d_{5/2}$ and $3d_{3/2}$ lines at 368.2 and 374.2 eV, respectively.[65] Total energy resolution of the measurement condition was estimated to be 0.9 eV from the full width of the Ag $3d_{5/2}$ line of 1.0 eV.[14] Samples did not show any radiation damage during XPS measurements.

An XPS peak-fitting analysis was performed with the Voigt functions and the Shirley background. Lorentzian widths of N 1s were set to 0.84 and 0.50 eV for the multilayer and monolayer samples, respectively.[19] The N 1s X-ray photoelectron spectra of $H_2Pc$ and VPc on Ag(111) were obtained by subtracting the spectrum of the clean substrate from those of $H_2Pc$ and VPc as well as from those of VOPc,[14] because the XPS N 1s region overlapped with the plasmon loss peaks of Ag(111).[66]

XAS and XMCD measurements were conducted on a 3 ML Ag film grown on Cu(111) as substrate to reduce the Ag background signals. Cu(111) was cleaned by repeated cycles of Ar ion sputtering and annealing at 800 K. Next Ag was deposited in a layer-by-layer manner at RT on the Cu. The thickness of Ag was estimated to be 3 ML from the AES intensities of Cu MVV. As reported previously,[67] the (9 × 9) superstructure was observed by LEED. Note here that Ag(3 ML)/Cu(111) shows an almost equivalent electronic structure to a Ag(111) single crystal. It is well-known that face-centered cubic (fcc) (111) surfaces exhibit specific surface states and that binding energy of the surface state in Ag/Cu(111) decreases with Ag thickness. The difference of binding energies of the surface state between Ag(3 ML)/Cu(111) and Ag(111) has been reported as ∼50 meV, which is 6 times smaller than that between Ag(111) and Cu(111) (∼300 meV).[68] Moreover, the self-assembled structure of a porphyrin film deposited on Ag(3 ML)/Cu(111) is found to be the same as that on Ag(111).[69] These previous remarks indicate that the interfacial interaction of VPc with Ag(3 ML)/Cu(111) may be almost identical to that with a Ag(111) single crystal.

VPc monolayers and multilayers for XAS and XMCD measurements were prepared according to the same procedures as XPS sample preparation. Additionally, a VPc monolayer was prepared on an $H_2Pc$ film (3 ML) formed on Ag/Cu(111) and covered by 1 ML $H_2Pc$ to investigate the absence of interaction between central V and substrate or between V ions in the upper and lower layers.

XAS and XMCD measurements were performed on an XMCD system ($P < 1 \times 10^{-8}$ Pa) equipped with a 7 T superconducting magnet and a liquid He cryostat ($T$ = 3.8 K) at the end station of the bending magnet beamline 4B of UVSOR-III (Institute for Molecular Science, Okazaki, Japan). This XMCD measurement system has been detailed previously.[70,71] Linearly polarized XAS measurements in the N K-edge and V $L_{2,3}$-edge regions were conducted at incident angles $\theta$ of 0°, 30°, and 55° with respect to the surface normal at a temperature of 5 K. The photon energy in each spectrum was set by use of identical features in N and O K-edge regions, which originate from contaminations in the beamline optics. X-ray energies were calibrated by use of the metallic V $L_3$ and $L_2$ peaks at 512.1 and 519.8 eV, respectively. The nominal energy resolution ($E/\Delta E$) of the linearly polarized X-rays in the N K-edge region was estimated as 2000 for 10 ML samples and 1300 for the other samples, and those in the V $L_{2,3}$-edge and O K-edge regions were 2000 for 10 ML samples and 1000 for the other samples. Circularly polarized XAS measurements at the V $L_{2,3}$ and O K edges were performed in a magnetic field of ±5 T at incident angles $\theta$ of 0° and 55° at a temperature of 5 K. The magnetic field was applied to the sample along the parallel and antiparallel directions with respect to the X-ray beam. XMCD spectra were obtained by subtracting $\mu^-$ from $\mu^+$. Here, $\mu^+$ ($\mu^-$) represents the applied magnetic field antiparallel (parallel) to the helicity of the X-rays. The estimated degree of circular polarization of the X-rays was approximately 0.6 from the beamline parameter. The $E/\Delta E$ value of the circularly polarized X-rays in the V $L_{2,3}$-edge and O K-edge regions was set to 1000 for 10 ML samples and 600 for the other samples. All XAS and XMCD spectra were recorded in the total electron yield detection (TEY) mode, and several spectral scans were averaged to enhance the signal-to-noise ratio. TEY spectra from the sample ($I_{sample}$) were divided by that of the clean substrate ($I_{subst}$). Here, these signals were first divided by the $I_0$ signals recorded with an Au mesh in the upstream of the sample. Note that the resultant normalized spectrum $\mu$ is thus given as $\mu = [I_{sample}/I_0]/[I_{subst}/I_0]$. No significant beam damage was observed although the synchrotron radiation typically lasted more than 10 h.

## 3. RESULTS AND DISCUSSION

**3.1. Direct Synthesis of VPc.** Metalation of $H_2Pc$ on a substrate is an excellent MPc synthetic technique. The formation of MPc can be confirmed by X-ray spectroscopy because $H_2Pc$ and MPc exhibit a remarkable difference in electronic states in the N 1s region.[30] Therefore, N 1s X-ray photoelectron spectra were determined for $H_2Pc$ and VPc samples.

Figure 2 shows N 1s X-ray photoelectron spectra for $H_2Pc$ and VPc monolayers. Two main peaks at 398.4 and 400.1 eV and one satellite peak at approximately 402.5 eV were observed for $H_2Pc$, which is in good agreement with previous reports.[30,72,73] According to the computational results,[72] the


DOI: 10.1021/jp512935v
J. Phys. Chem. C 2015, 119, 9805−9815

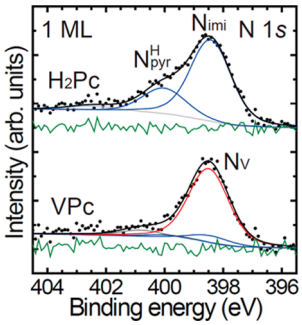


**Figure 2.** N 1s X-ray photoelectron spectra of 1 ML $H_2Pc$ and VPc taken at room temperature. The components of $N_{imi}$ and $N^{H}_{pyr}$ in $H_2Pc$ and $N_V$ in VPc in the main peaks are shown by blue and red lines, respectively. Shake-up satellite peaks at approximately 402.5 eV in $H_2Pc$ and approximately 401 eV in VPc appear as gray lines. Green lines represent peak fitting residues.

main peaks at 398.4 and 400.1 eV were assigned to iminic (−N═, $N_{imi}$) and pyrrolic N atoms (−NH−, $N^{H}_{pyr}$), respectively. Although two different peaks corresponding to iminic N atoms were expected on each side of the $N_{imi}$ peak in $H_2Pc$, the peak fitting was performed as a single contribution because the energy difference only equaled 0.4 eV.[72] The $N_{imi}/N^{H}_{pyr}$ ratio amounted to 2.99, consistent with the stoichiometry of $H_2Pc$. The peak at approximately 402.5 eV was attributed to the shakeup satellite.[73]

After V deposition on $H_2Pc$ at RT, the $N^{H}_{pyr}$ peak intensity decreased drastically, while a main peak at 398.5 eV and a satellite peak at approximately 401 eV were observed in the N 1s spectrum. Here, the peak fitting was performed by assuming that the peak at 400.1 eV is the component of $H_2Pc$ and the intensity ratio $N_{imi}/N^{H}_{pyr}$ is fixed at 3.00, because it is hard to separate the components of $N_V$ in VPc and $N_{imi}$ in $H_2Pc$ due to the low energy resolution of the experimental system. The spectrum presented a very similar shape to that of MPcs, such as TiOPc,[74] VOPc,[13,14] FePc,[30] and CuPc,[75] clearly implying that the deposited V was coordinated by the phthalocyanine ligand and N−V bonds formed between V and the inner N atoms. The contribution of all N atoms in VPc ($N_V$, see Figure 1b) to the total intensity of the N 1s spectrum equaled 0.88 after peak fitting. Therefore, it is found that $H_2Pc$ easily reacted with the deposited V without annealing, unlike the direct synthesis of Zn porphyrin, which required annealing.[25]

Although the metalation of $H_2Pc$ occurs readily for VPc and FePc[30] monolayers, the metalation of multilayers usually proceeds with difficulty when metallic atoms are deposited on $H_2Pc$ multilayers.[30] Therefore, the VPc multilayer (10 ML) was prepared by repeating the VPc monolayer synthesis 10 times to solve this problem. Figure 3 shows the N 1s X-ray photoelectron spectra of the 10 ML film. Similar to the $H_2Pc$ monolayer, two peaks corresponding to $N_{imi}$ (398.6 eV) and $N^{H}_{pyr}$ (400.2 eV) were detected in this N 1s spectrum, in addition to a satellite peak (~402.5 eV). The $N^{H}_{pyr}$ peak intensity decreased concomitant with the appearance of the $N_V$ peak for the as-deposited VPc multilayer. However, the ratio between the $N_V$ peak intensity and the total N 1s peak intensity amounted to 0.61. Furthermore, the appearance of a new $N_X$ peak was confirmed by peak fitting, although the origin of this peak was unclear (it might be a V−NH state but we could not identify its origin). Therefore, VPc partially formed in the multilayer but the quality of the film was insufficient. Here, the peak fitting was performed in a similar manner to the case of

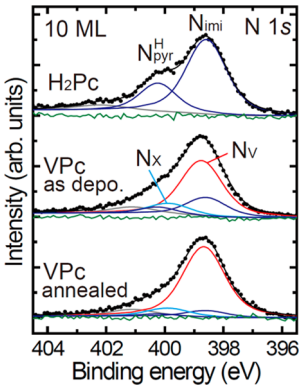


**Figure 3.** N 1s X-ray photoelectron spectra of 10 ML $H_2Pc$ and VPc multilayers (10 ML) taken at room temperature. Spectra of VPc before and after annealing are shown at the center and bottom, respectively. Components of $N_{imi}$ and $N^{H}_{pyr}$ in $H_2Pc$ and $N_V$ in VPc in the main peaks are represented by dark blue and red lines, respectively. Light blue lines correspond to the unidentified peak $N_X$. Shake-up satellite peaks at approximately 402.5 eV in $H_2Pc$ and approximately 401 eV in VPc appear as gray lines. Green lines indicate peak fitting residues.

the VPc monolayer; namely, we assumed that the peak at 400.2 eV originates from $H_2Pc$ and the intensity ratio $N_{imi}/N^{H}_{pyr}$ is 3.00. The $N_X$ peak was used to give a reasonable fit because no convincing fit was obtained without the $N_X$ peak. To promote the reaction of V with $H_2Pc$ and the quality of the VPc film, the sample was annealed at ~450 K. Annealing further reduced the intensity of the $N^{H}_{pyr}$ peak and enhanced that of the $N_V$ peak for the VPc multilayer. The $N_V$ peak intensity corresponded to 81% of the total N 1s XPS intensity, suggesting that annealing enhanced the VPc film quality.

XPS measurements were also performed in the V 2p region to investigate the oxidation state of the central V in VPc monolayer and multilayer. Figure 4a shows the V 2p X-ray photoelectron spectra for VPc monolayer, as-deposited and annealed VPc multilayers (10 ML), and VOPc multilayer (10 ML) acting as a reference. The oxidation state of V in VPc can be estimated from the V $2p_{3/2}$ peak position.[76−84] The VOPc multilayer displayed a quadrivalent formal oxidation state for V and a V $2p_{3/2}$ binding energy of 516.4 eV, which is close to that of V(IV) in $VO_2$ (Figure 4b). The annealed VPc multilayer exhibited a V $2p_{3/2}$ peak at 514.8 eV, representing a lower energy than that for V(III) in $V_2O_3$ but higher energy than that for metallic V. The oxidation state of V in the VPc multilayer was thus expected to be smaller than trivalent. Furthermore, if a linear relationship between the oxidation state of V and the binding energy of V 2p is assumed, the nominal oxidation state of V in the VPc multilayer was estimated as 2.4 at the intersection of the line and the V binding energy. Here a straight line was obtained by connecting the average binding energies of V in the metal and in VOPc, and the standard deviation of the binding energies of 0.14 eV for V(0) might give an estimated error of ±0.12 in the oxidation states of V. This result supports the formation of VPc. In addition, the peak of the as-deposited multilayer at approximately 513 eV reduced drastically in the annealed sample and shifted toward higher binding energy upon annealing. This means that the annealing process accelerates VPc formation, consistent with the N 1s XPS results.

In the VPc monolayer, the peak position was estimated to be 513.9 eV by peak fitting (see Figure 4a). The peak showed a shift of 0.9 eV lower than the binding energy of VPc multilayer,


DOI: 10.1021/jp512935v
J. Phys. Chem. C 2015, 119, 9805−9815

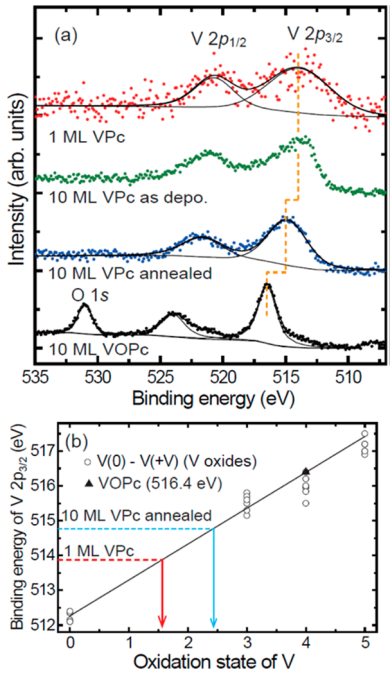


**Figure 4.** (a) V 2p and O 1s X-ray photoelectron spectra of VPc monolayer, VPc multilayer before and after annealing, and VOPc multilayer at room temperature. V 2p spectra were split into $2p_{3/2}$ and $2p_{1/2}$ because of spin−orbit interactions. Experimental data are shown as dots, while fitting curves are represented by black lines. The guide lines indicating peak positions are shown in orange. (b) Relationship between oxidation state of V and binding energy of V $2p_{3/2}$ in XPS. The triangle corresponds to the binding energy of VOPc obtained in this study. Circles represent the reported binding energies of clean V metal and vanadium oxides.[76−84] The binding energy of V $2p_{3/2}$ in VPc monolayer and multilayer are shown by red and blue dashed lines, respectively.

and the nominal oxidation state of V in this monolayer was estimated as 1.6 by using the relationship between oxidation state and binding energy (Figure 4b). The XPS peak shift of the metal center was also observed in phthalocyanine or porphyrin systems, such as MnPc,[85] FePc,[30,86] CoPc/Ag(111),[85] CoTPP/Ag(111),[16,87,88] CoPc on polycrystalline Au,[89] FePc,[86] ZnPc/Au(100),[90] CuPc/Al(100),[91] ZnPc/Pt(111),[92] MgPc on the Au foil,[93] and PbPc/Ag(111).[94] Spectroscopic methods have suggested that the shift toward lower binding energies originates from charge-transfer effects. Although the contribution of the polarization screening effect is also expected, the effect has been clarified to be considerably smaller than the charge-transfer screening effect in ZnPc and MgPc on Au systems.[90,93] The charge-transfer effects generally depend on a combination of adsorbed molecules with metal substrates. The V $2p_{3/2}$ line of the VPc monolayer shows a 0.9 eV shift, which is relatively smaller than those of FePc (1.5 eV)[30,86] and CoPc (1.8 eV)[85] on Ag(111), CoPc (∼1.6 eV) on Au,[95] and CuPc (1.6 eV) on Al(100).[91] Interaction of the VPc monolayer with the Ag surface is thus expected to be as weak as that for MnPc on Ag(111),[85] which may result from the small electron affinity of the metal center. The shift of binding energy also originates from the final-state charge-transfer (relaxation) effect. As shown in the next section, however, a similar peak shift is observed in X-ray absorption spectra of the VPc monolayer on Ag, where the final-state relaxation effect should be smaller due to the existence of the excited electron within the V orbitals. This indicates that the final-state relaxation effect is less important for the shift of the XPS binding energy and that charge transfer in the initial state should be a major contribution to the shift of the binding energy.

C 1s XPS measurements were also conducted for $H_2Pc$ and VPc monolayers and multilayers (see Supporting Information). When the spectra of 10 ML VPc and 10 ML $H_2Pc$ are compared, the benzene C peak of VPc shifts 0.2 eV toward a higher binding energy side, although no peak shift was observed in that of pyrrole C. On the other hand, the shifts of benzene C and pyrrole C of the VPc monolayer are 0.1 and 0.3 eV, respectively, in comparison with those of $H_2Pc$. In addition, both benzene and pyrrole C in the VPc monolayer appear at a lower binding energy side (0.3 eV), compared with those in the VPc multilayer. Thus, we observed site-specific chemical shifts.

In summary, VPc monolayer and multilayer were directly synthesized by deposition of $H_2Pc$ molecules and V atoms on Ag(111) under UHV conditions. The VPc monolayer was obtained by V deposition on the self-assembled $H_2Pc$ monolayer without sample annealing. On the other hand, the metalation reaction alone was insufficient for the 10 ML sample but was promoted by annealing, leading to the VPc multilayer.

**3.2. Electronic Configuration and Magnetic States of VPc.** Angle-dependent linearly polarized XAS measurements, which typically provide molecular orientation and unoccupied orbitals,[33,96−98] were performed to elucidate the electronic configuration of the central V in VPc. Furthermore, XMCD measurements were conducted with circularly polarized X-rays to investigate the magnetic properties of VPc. In addition, the magnetic property of a VPc monolayer embedded in an $H_2Pc$ film (see Experimental Section) was also investigated to clarify the interfacial interaction between VPc and the Ag surface and the intermolecular interaction between VPc molecules in neighboring layers. All XAS and XMCD measurements were performed at 5 K because ferromagnetic or antiferromagnetic states of MPcs (M = Mn,[56] Fe,[44] and Co[42]) have interestingly been observed at low temperature. Although the vibration of molecules is suppressed at low temperature, no structural change is expected in this temperature region.

The molecular orientation of VPc in monolayers and multilayers was first investigated to determine the electronic configuration of the central V. Angle-dependent N K-edge X-ray absorption spectra is shown in Figure 5. The spectrum of VPc exhibited at least eight peaks (A−H), similar to those of other MPcs.[14,98−100] Here, we notice that VPc provides two peaks (peaks C and D) in the energy region between 401 and 405 eV, although 10 ML $H_2Pc$ gives three peaks (see Supporting Information) in this region. This difference between nonmetallic and metal phthalocyanines has been also observed in other MPcs (M = $H_2$, Fe, Co, and Cu),[98] supporting the formation of VPc. On the other hand, we could not detect a reliable difference between X-ray absorption spectra of VPc and $H_2Pc$ monolayers (see Supporting Information). In addition, a bump structure at ∼403 eV in the spectrum of the VPc monolayer at 55° (green arrow in Figure 5) might be an artifact originating from incomplete elimination of the contamination effect on the beamline optics in the spectral normalization process ($I/I_0$) due to small signals from the monolayer sample. Peaks A−D were mainly attributed to N 1s → $\pi^*$ molecular orbital transitions, and peaks E−H corresponded to transitions involving $\sigma^*$ resonances.[98,99,101] In $\pi$-conjugated molecular systems, the transition from 1s to a p-type molecular orbital is most intense when an electric field vector of linearly polarized


DOI: 10.1021/jp512935v
J. Phys. Chem. C 2015, 119, 9805−9815

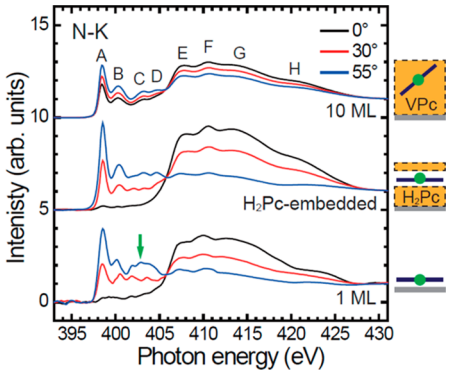


**Figure 5.** Angle-dependent linearly polarized X-ray absorption spectra at the N K edge for VPc multilayer, $H_2Pc$-embedded VPc monolayer, and VPc monolayer on Ag(111). The green arrow indicates an artifact bump structure. Measurements were performed at 5 K. The energy resolution ($E/\Delta E$) amounted to 2000 for the VPc multilayer and $H_2Pc$-embedded VPc and 1300 for the VPc monolayer.

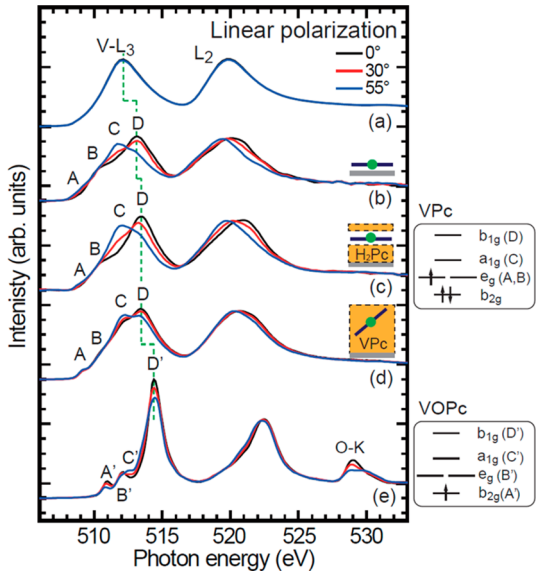


**Figure 6.** Angle-dependent linearly polarized X-ray absorption spectra at V $L_{2,3}$ edge and O K edge for (a) metallic V, (b) VPc monolayer, (c) $H_2Pc$-embedded VPc monolayer, (d) VPc multilayer, and (e) VOPc multilayer. Peak positions are represented by green dashed lines. Measurements were conducted at 5 K. The energy resolution ($E/\Delta E$) equaled 2000 for metallic V and VPc and VOPc multilayers and 1000 for VPc monolayers. Molecular orientation of VPc is schematically shown inside the graph for spectra b–d. Schematic energy diagrams of V 3d orbitals in VPc and VOPc are shown in insets to the right. Peaks A, B, C, and D (A′, B′, C′ and D′) correspond to $e_g$, $a_{1g}$, and $b_{1g}$ ($b_{2g}$, $e_g$, $a_{1g}$, and $b_{1g}$) orbitals, respectively, in VPc (VOPc).

X-rays points in the direction of the unoccupied orbital, and no transition occurs when the vector is perpendicular to the orbital.[96,97] The $\pi^*$ peak intensity of the VPc monolayer was extremely weak at an incident X-ray angle of 0° and increased when the X-ray electric field vector was gradually tilted away from the surface, indicating that the phthalocyanine framework lay flat with respect to the surface. Similarly, the $\pi^*$ intensity of the $H_2Pc$-embedded VPc monolayer was small at 0° and increased with the incident X-ray angle. Therefore, VPc was adsorbed in a flat orientation with respect to the surface even though the signals originating from the upper and lower layers of the $H_2Pc$ film were also included in the spectra. On the other hand, the $\pi^*$ intensity of the VPc multilayer was large at 0° and displayed smaller angular dependence, meaning that VPc was tilted with respect to the surface in the upper side of the film. This result might imply the unreacted V disturbs the adsorption of $H_2Pc$ overlayer with flat orientation. The estimated molecular orientation was 40° with respect to the substrate surface, calculated from the maximum intensity ratio between $I_{0°}$ and $I_{55°}$ (0.63).[97] This angle is close to that observed in the $\beta$ phase.[42]

Angle-dependent V L-edge X-ray absorption apectra of VPc, metallic V, and VOPc are shown in Figure 6. All spectra were split into $L_3$ and $L_2$ regions because of the spin–orbit interactions in the V 2p orbitals. In agreement with the XPS results, the V L-edge XAS peak position correlated linearly with the oxidation state of V,[102] enabling an estimate of the oxidation state of V in VPc. Here, this estimate used the main peak position for the V $L_3$ edge, and the V metal peak position was assumed to be 512.1 eV. The VOPc multilayer (10 ML) and VPc monolayer peaks appeared at 514.4 and 513.1 eV, respectively, while the VPc multilayer and $H_2Pc$-embedded VPc monolayer exhibited a peak at 513.4 eV. With the assumption that V displayed formal oxidation states of 0 and +4 in the metal and VOPc, respectively, its oxidation state was estimated to be +2.3 for the VPc multilayer and the $H_2Pc$-embedded VPc monolayer and +1.7 for the VPc monolayer, which were in good agreement with the XPS estimates.

Next, angle-dependent V L-edge X-ray absorption spectra and their characteristics were addressed. Metallic V exhibited broad XAS peaks and no angular dependence with respect to the incident X-ray. On the other hand, XAS presented fine structures assigned to peaks A–D (A′–D′) and angular dependence for VPc (VOPc). These angular dependences provide the unoccupied 3d orbitals in the films. Peaks A′–D′ observed for VOPc have been previously attributed to transitions from V 2p cores to $b_{2g}$, $e_g$, $a_{1g}$, and $b_{1g}$ orbitals, respectively.[14] The peak assignment for VPc was conducted with the X-ray absorption spectrum of $H_2Pc$-embedded VPc monolayer because of its clear angular dependence. In this case, the $b_{1g}$ and $b_{2g}$ orbitals were spread parallel to the surface, while the $a_{1g}$ orbital is perpendicular to the surface, because VPc adsorbs in flat orientation with respect to the surface. The main peak D clearly showed angular dependence. Its intensity was maximized at 0° and decreased with increasing incident X-ray angle. Peak D was located at a higher energy than the other peaks, enabling its attribution to $b_{1g}$. This is in accordance with the previous observations for MnPc,[57,85] FePc,[86,103] and CoPc.[85,103] In addition, this result excludes the possibility of the formation of a double-decker structure because the $b_{1g}$ and $b_{2g}$ orbitals are expected to be degenerate in the double-decker structure. In contrast, the intensity of peak C increased with rising incident X-ray angle, suggesting its assignment to $a_{1g}$. This intensity was almost the same as that of peak D, indicating that the $a_{1g}$ orbital was unoccupied. Peaks A and B display little angular dependence and appear at a lower photon energy side than peaks C and D, implying that peaks A and B can be assigned to the $e_g$ orbital and its energy level was lower than those of $b_{1g}$ and $a_{1g}$ orbitals. Furthermore, the transition to $b_{2g}$ (peak A′) observed in the X-ray absorption spectrum of VOPc was not detected in that of VPc. Therefore, the $b_{2g}$ orbital of V in VPc was expected to be fully occupied and an unpaired electron may occupy the $e_g$ orbital, suggesting that the electronic configuration of V in VPc corresponded to $^2E_g$ ($b_{2g}^2$ $e_g^1$ $a_{1g}^0$ $b_{1g}^0$). Therefore, the lowest 3d level in VPc was


DOI: 10.1021/jp512935v
J. Phys. Chem. C 2015, 119, 9805–9815

$b_{2g}$, in agreement with previous results obtained for other MPc systems.[46,57,103] VPc was expected to display a spin state of $^1/_2$ as a result of the electronic state of V.

XMCD measurements were performed at 5 K for these three samples to investigate the magnetic properties of VPc. Circularly polarized XAS and XMCD spectra of VPc are shown in Figure 7a–c. Those of VOPc are also shown in Figure

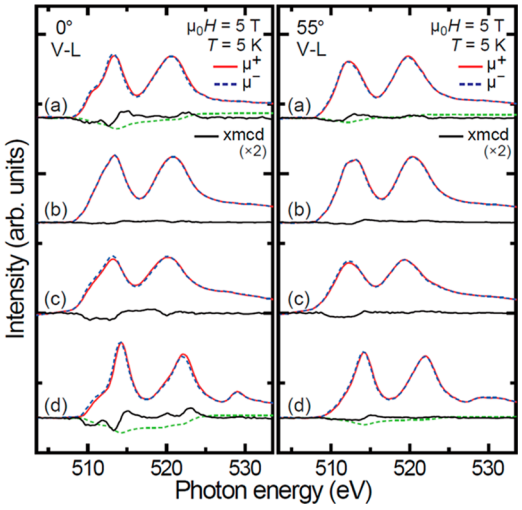


**Figure 7.** Circularly polarized XAS (red and blue lines) and XMCD spectra (black lines) at the V L edge of (a) $H_2$Pc-embedded VPc monolayer, (b) VPc multilayer, (c) VPc monolayer, and (d) VOPc monolayer in a magnetic field of ±5 T at 5 K and incident X-ray angles of 0° (normal incidence) and 55° (grazing incidence). All XMCD signals were magnified twice. Green dashed lines represent the integrals of the XMCD signals from 507 to 527 eV. The energy resolution ($E/\Delta E$) of the circularly polarized X-rays in V $L_{2,3}$-edge and O K-edge regions was set to 1000 for multilayers and 625 for the other samples.

7d as references for paramagnetic V exhibiting an $S$ value of $^1/_2$. The magnetic interaction between the central V was ignored in the $H_2$Pc-embedded VPc monolayer because VPc was sandwiched between the $H_2$Pc layers and the distance between neighboring V ions in the layer might be close to 1.4 nm in the flat orientation. XMCD spectra of the $H_2$Pc-embedded VPc monolayer presented explicit signals at incident angles of 0° and 55°. The XMCD signal of the $H_2$Pc-embedded VPc at 0° displays almost the same intensity as that of the VOPc monolayer. Therefore, the spin state of the $H_2$Pc-embedded VPc was considered to be $^1/_2$, consistent with the electronic state suggested from the linearly polarized XAS measurements. The orbital magnetic moment of VPc was approximately twice that of VOPc, as obtained by the integration of XMCD signals at $L_3$ and $L_2$ edges (green dashed lines, Figure 7). Because the orbital magnetic moment of VOPc amounted to ca. $0.02\mu_B$,[12,104] that of VPc was expected to be approximately $0.04\mu_B$, although the $E_g$ configuration of a divalent V ion predicts a much larger orbital magnetic moment of $1\mu_B$, implying quenching of the orbital magnetic moment by formation of the VPc complex. This discrepancy may result from the significant contribution of the covalent bond (overlapping) between V $3d_\pi$ and N $2p_\pi$ in VPc. However, this explanation may be insufficient. The proposed $^2E_g$ state contributed to the electronic structure of VPc to a great extent but did not completely describe its ground-state electronic configuration. This suggests that a spin–orbit configuration interaction occurred between $^2E_g$ and $^2A_{1g}$ ($b_{2g}^2$ $e_g^0$ $a_{1g}^1$ $b_{1g}^0$) states because $^2A_{1g}$ exhibits no orbital magnetic moment. This interpretation of the ground state is consistent with the previous reports for FePc[105] and CoPc.[41,105] In these previous systems, FePc and CoPc ground states were expressed as $^3B_{2g}$–$^3E_g$ and $^2A_{1g}$–$^2E_g$ mixed states, respectively. The ground state of V in VPc was also expected to be the $^2E_g$–$^2A_{1g}$ mixed state and its small orbital magnetic moment might have resulted from the covalent bond character and configuration interaction with the $^2A_{1g}$ state. The Jahn–Teller effect may also reduce the orbital magnetic moment but was not very effective for the $H_2$Pc-embedded VPc monolayer because of the rigid phthalocyanine ligand.

The XMCD signals of V decreased drastically for the VPc multilayer, indicative of the antiferromagnetic state of VPc in this sample as a result of the antiferromagnetic interaction between VPc in the upper and lower layers. The magnetic interaction in the multilayer agrees with the previous observation in antiferromagnetic $\alpha$-CoPc[42] and $\beta$-CoPc[106] as well as ferromagnetic $\alpha$-FePc[44,47] and $\beta$-MnPc.[54,58] Here, the possible antiferromagnetic coupling of VPc was addressed by assuming that the VPc multilayer adopts a $\beta$ structure (metal–metal distance of 4.8 Å)[107] from the molecular orientation of the multilayer film. In this case, the $e_g$ orbital of the V center pointed toward other V centers in the upper and lower layers. This made the direct overlap of the V center half-filled $e_g$ orbitals possible, leading to antiferromagnetism.[108] Additionally, antiferromagnetic interactions between the ferromagnetic VPc chains may also exist but their contributions may be negligible because the distance between VPc chains exceeded approximately 1 nm, which is estimated by assuming a lateral molecular distance of 1.4 nm in the flat orientation and a tilt angle of 42.9° in the $\beta$ phase (of CoPc),[42] and the interchain interaction was estimated to be less than 2 K, as suggested by previous reports on the magnetic properties of CuPc[109] and FePc[44] films.

Finally, the interaction between VPc and Ag surface was investigated. A comparison between X-ray absorption spectra of VPc monolayer and $H_2$Pc-embedded VPc revealed that peak D appeared at a lower photon energy for the 1 ML sample (see Figure 6). In addition, the VPc monolayer produced broader XAS peaks than $H_2$Pc-embedded VPc. These suggest that charge transfer occurred from the Ag surface to the V center and the produced 2p core hole in V displayed a short lifetime at the VPc–Ag interface. The charge-transfer effect has also been observed in other MPc systems deposited on metallic substrates, and the transition intensities decreased by occupation of the 3d orbitals.[46,85,86,105] The intensity of peak C decreased for VPc, indicating the important role of the $a_{1g}$ orbital in the electron charge transfer and the formation of a hybridized state with the Ag surface. However, this reduction in peak intensity was not significant compared with CoPc/Ag(111),[85] FePc/Ag(111),[86] and MnPc/Au(100).[57] Moreover, the peak intensities related to the $b_{1g}$ orbital diminished in CoPc/Ag(111),[85] FePc/Ag(111),[86] and MnPc/Au(100).[57] In contrast, no clear reduction in peak D ($b_{1g}$) was observed in VPc/Ag(111), as for CuPc/Au(110).[46] Despite the existence of charge transfer in VPc/Ag(111), this charge transfer was not very effective from the Ag surface to V.

XMCD results were examined to get an insight into the influence of interface interactions on VPc magnetic properties. Figure 7c shows the XMCD signals of VPc monolayer, and Figure 7a shows those of $H_2$Pc-embedded VPc. The VPc


DOI: 10.1021/jp512935v
J. Phys. Chem. C 2015, 119, 9805–9815

monolayer displayed slightly weaker signals than $H_2Pc$-embedded VPc, consistent with the XMCD data for CuPc/Au(110)[46] and MnPc/Cu(001).[110] However, this result disagrees with the XMCD signals obtained for CoPc/Au(111),[105] CoPc/Au(110),[46] and FePc/Au(110),[46] which decreased dramatically and indicated the disappearance of the spin(s). The XMCD intensity of V decreased at the VPc/Ag(111) interface, but this signal reduction was not significant because of the insufficient charge-transfer effect and the small electron affinity of V as compared to Fe and Co.

## 4. SUMMARY

It is not straightforward to study the electronic and magnetic states of early transition metal phthalocyanines because their instability to air makes the development of synthetic procedures challenging. To overcome this issue, VPc was directly synthesized on an Ag surface under UHV conditions. After V deposition on the $H_2Pc$ monolayer film, the XPS peak ascribed to the H-bonded N atoms clearly decreased, while a new peak assigned to the V−N bond formation appeared. Similar peak changes were observed in the VPc multilayer, although it required subsequent annealing after the deposition of V. UHV conditions protected the V ions from oxidation and the oxidation state of V was divalent, demonstrating the successful synthesis of VPc on the Ag surface. This also made investigations of the electronic and magnetic states of VPc possible.

These electronic and magnetic states were evaluated by XAS and XMCD measurements under UHV conditions. The electronic configuration of the V ion in VPc was mainly attributed to $^2E_g$ by angle-dependent XAS. Although this $^2E_g$ configuration satisfied a spin state of $^1/_2$, the small orbital magnetic moment obtained by XMCD was difficult to interpret. Mixed configurations involving $^2E_g$ and $^2A_{1g}$ resulting from spin−orbit coupling were consequently suggested for the ground state of VPc. The $b_{2g}$ orbital displayed the lowest energy level and was occupied in VPc. VPc showed paramagnetic behavior in the $H_2Pc$-embedded VPc system while it formed an antiferromagnetic state in the VPc multilayer as a result of antiferromagnetic interaction between the layers. The VPc/Ag interface exhibited charge transfer from the Ag surface to V, similar to other divalent MPcs deposited on metal substrates. The XMCD signals persisted at the interface, unlike for CoPc on Au(111)[105] and Au(110).[46]

## ■ ASSOCIATED CONTENT

### Supporting Information

Additional text and two figures showing C 1s XPS and N K-edge XAS spectra of VPc and $H_2Pc$ monolayers and multilayers; complete refs 29, 46, 58, 72, and 110. The Supporting Information is available free of charge on the ACS Publications website at DOI: 10.1021/jp512935v.

## ■ AUTHOR INFORMATION

### Corresponding Author

*E-mail yokoyama@ims.ac.jp; phone +81 (564)55 7341; fax +81 (564)55 7337.

### Notes

The authors declare no competing financial interest.

## ■ ACKNOWLEDGMENTS

We thank Professor Fujikawa, Dr. Matsunami, and Dr. Yamane for their helpful discussions.

## ■ REFERENCES

(1) Moser, F. H.; Thomas, A. L. *The Phthalocyanines: Properties*; CRC Press: Boca Raton, FL, 1983.
(2) Bohrer, F. I.; Colesniuc, C. N.; Park, J.; Ruidiaz, M. E.; Schuller, I. K.; Kummel, A. C.; Trogler, W. C. Comparative Gas Sensing in Cobalt, Nickel, Copper, Zinc, and Metal-Free Phthalocyanine Chemiresistors. *J. Am. Chem. Soc.* **2008**, *131*, 478−485.
(3) Peumans, P.; Yakimov, A.; Forrest, S. R. Small Molecular Weight Organic Thin-Film Photodetectors and Solar Cells. *J. Appl. Phys.* **2003**, *93*, 3693−3723.
(4) Hains, A. W.; Liang, Z.; Woodhouse, M. A.; Gregg, B. A. Molecular Semiconductors in Organic Photovoltaic Cells. *Chem. Rev.* **2010**, *110*, 6689−6735.
(5) Yamane, H.; Kosugi, N. Substituent-Induced Intermolecular Interaction in Organic Crystals Revealed by Precise Band-Dispersion Measurements. *Phys. Rev. Lett.* **2013**, *111*, No. 086602.
(6) Schmaus, S.; Bagrets, A.; Nahas, Y.; Yamada, T. K.; Bork, A.; Bowen, M.; Beaurepaire, E.; Evers, F.; Wulfhekel, W. Giant Magnetoresistance through a Single Molecule. *Nat. Nanotechnol.* **2011**, *6*, 185−189.
(7) Urdampilleta, M.; Klyatskaya, S.; Cleuziou, J. P.; Ruben, M.; Wernsdorfer, W. Supramolecular Spin Valves. *Nat. Mater.* **2011**, *10*, 502−506.
(8) Myers, J. F.; Canham, G. W. R.; Lever, A. B. P. Higher Oxidation Level Phthalocyanine Complexes of Chromium, Iron, Cobalt and Zinc. Phthalocyanine Radical Species. *Inorg. Chem.* **1975**, *14*, 461−468.
(9) Kasuga, K.; Tsutsuo, M. Some New Developments in the Chemistry of Metallophthalocyanines. *Coord. Chem. Rev.* **1980**, *32*, 67−95.
(10) Ejsmont, K.; Kubiak, R. Iodo(Phthalocyaninato)Vanadium(III). *Acta Crystallog., Sect. C: Cryst. Struct. Commun.* **1998**, *54*, 1844−1846.
(11) Griffiths, C. H.; Walker, M. S.; Goldstein, P. Polymorphism in Vanadyl Phthalocyanine. *Mol. Cryst. Liq. Cryst.* **1976**, *33*, 149−170.
(12) Assour, J. M.; Goldmacher, J.; Harrison, S. E. Electron Spin Resonance of Vanadyl Phthalocyanine. *J. Chem. Phys.* **1965**, *43*, 159.
(13) Zhang, Y.; Learmonth, T.; Wang, S.; Matsuura, A. Y.; Downes, J.; Plucinski, L.; Bernardis, S.; O'Donnell, C.; Smith, K. E. Electronic Structure of the Organic Semiconductor Vanadyl Phthalocyanine (VO-Pc). *J. Mater. Chem.* **2007**, *17*, 1276.
(14) Eguchi, K.; Takagi, Y.; Nakagawa, T.; Yokoyama, T. Molecular Orientation and Electronic States of Vanadyl Phthalocyanine on Si(111) and Ag(111) Surfaces. *J. Phys. Chem. C* **2013**, *117*, 22843−22851.
(15) Eguchi, K.; Takagi, Y.; Nakagawa, T.; Yokoyama, T. Magnetic Interactions of Vanadyl Phthalocyanine with Ferromagnetic Iron, Cobalt, and Nickel Surfaces. *J. Phys. Chem. C* **2014**, *118*, 17633−17637.
(16) Gottfried, J. M.; Flechtner, K.; Kretschmann, A.; Lukasczyk, T.; Steinrück, H.-P. Direct Synthesis of a Metalloporphyrin Complex on a Surface. *J. Am. Chem. Soc.* **2006**, *128*, 5644−5645.
(17) Buchner, F.; Schwald, V.; Comanici, K.; Steinruck, H. P.; Marbach, H. Microscopic Evidence of the Metalation of a Free-Base Porphyrin Monolayer with Iron. *ChemPhysChem* **2007**, *8*, 241−243.
(18) Buchner, F.; Flechtner, K.; Bai, Y.; Zillner, E.; Kellner, I.; Steinrück, H.-P.; Marbach, H.; Gottfried, J. M. Coordination of Iron Atoms by Tetraphenylporphyrin Monolayers and Multilayers on Ag(111) and Formation of Iron-Tetraphenylporphyrin. *J. Phys. Chem. C* **2008**, *112*, 15458−15465.
(19) Di Santo, G.; Castellarin-Cudia, C.; Fanetti, M.; Taleatu, B.; Borghetti, P.; Sangaletti, L.; Floreano, L.; Magnano, E.; Bondino, F.; Goldoni, A. Conformational Adaptation and Electronic Structure of 2H-Tetraphenylporphyrin on Ag(111) during Fe Metalation. *J. Phys. Chem. C* **2011**, *115*, 4155−4162.


DOI: 10.1021/jp512935v
J. Phys. Chem. C 2015, 119, 9805−9815

(20) Auwarter, W.; Weber-Bargioni, A.; Brink, S.; Riemann, A.; Schiffrin, A.; Ruben, M.; Barth, J. V. Controlled Metalation of Self-Assembled Porphyrin Nanoarrays in Two Dimensions. *ChemPhysChem* **2007**, *8*, 250−254.
(21) Buchner, F.; Warnick, K.-G.; Wölfle, T.; Görling, A.; Steinrück, H.-P.; Hieringer, W.; Marbach, H. Chemical Fingerprints of Large Organic Molecules in Scanning Tunneling Microscopy: Imaging Adsorbate−Substrate Coupling of Metalloporphyrins. *J. Phys. Chem. C* **2009**, *113*, 16450−16457.
(22) Gottfried, J. M.; Marbach, H. Surface-Confined Coordination Chemistry with Porphyrins and Phthalocyanines: Aspects of Formation, Electronic Structure, and Reactivity. *Z. Phys. Chem.* **2009**, *223*, 53−74.
(23) Chen, M.; Feng, X.; Zhang, L.; Ju, H.; Xu, Q.; Zhu, J.; Gottfried, J. M.; Ibrahim, K.; Qian, H.; Wang, J. Direct Synthesis of Nickel(II) Tetraphenylporphyrin and its Interaction with a Au(111) Surface: A Comprehensive Study. *J. Phys. Chem. C* **2010**, *114*, 9908−9916.
(24) Wang, C.; Fan, Q.; Hu, S.; Ju, H.; Feng, X.; Han, Y.; Pan, H.; Zhu, J.; Gottfried, J. M. Coordination Reaction between Tetraphenylporphyrin and Nickel on a $TiO_2$(110) Surface. *Chem. Commun. (Cambridge, U. K.)* **2014**, *50*, 8291−8294.
(25) Kretschmann, A.; Walz, M. M.; Flechtner, K.; Steinruck, H. P.; Gottfried, J. M. Tetraphenylporphyrin Picks up Zinc Atoms from a Silver Surface. *Chem. Commun. (Cambridge, U. K.)* **2007**, 568−570.
(26) Shubina, T. E.; Marbach, H.; Flechtner, K.; Kretschmann, A.; Jux, N.; Buchner, F.; Steinrück, H.-P.; Clark, T.; Gottfried, J. M. Principle and Mechanism of Direct Porphyrin Metalation: Joint Experimental and Theoretical Investigation. *J. Am. Chem. Soc.* **2007**, *129*, 9476−9483.
(27) Ecija, D.; Auwarter, W.; Vijayaraghavan, S.; Seufert, K.; Bischoff, F.; Tashiro, K.; Barth, J. V. Assembly and Manipulation of Rotatable Cerium Porphyrinato Sandwich Complexes on a Surface. *Angew. Chem., Int. Ed.* **2011**, *50*, 3872−3877.
(28) Weber-Bargioni, A.; Reichert, J.; Seitsonen, A. P.; Auwarter, W.; Schiffrin, A.; Barth, J. V. Interaction of Cerium Atoms with Surface-Anchored Porphyrin Molecules. *J. Phys. Chem. C* **2008**, *112*, 3453−3455.
(29) Écija, D.; et al. Molecular Conformation, Organizational Chirality, and Iron Metalation of *meso*-Tetramesitylporphyrins on Copper(100). *J. Phys. Chem. C* **2008**, *112*, 8988−8994.
(30) Bai, Y.; Buchner, F.; Wendahl, M. T.; Kellner, I.; Bayer, A.; Steinruck, H.-P.; Marbach, H.; Gottfried, J. M. Direct Metalation of a Phthalocyanine Monolayer on Ag(111) with Coadsorbed Iron Atoms. *J. Phys. Chem. C* **2008**, *112*, 6087−6092.
(31) Schaffer, A.; Gouterman, M.; Davidson, E. Porphyrins XXviii. Extended Hückel Calculations on Metal Phthalocyanines and Tetrazaporphins. *Theor. Chim. Acta* **1973**, *30*, 9−30.
(32) Liao, M.-S.; Scheiner, S. Electronic Structure and Bonding in Metal Phthalocyanines, Metal = Fe, Co, Ni, Cu, Zn, Mg. *J. Chem. Phys.* **2001**, *114*, 9780.
(33) Kroll, T.; Kraus, R.; Schonfelder, R.; Aristov, V. Y.; Molodtsova, O. V.; Hoffmann, P.; Knupfer, M. Transition Metal Phthalocyanines: Insight into the Electronic Structure from Soft X-Ray Spectroscopy. *J. Chem. Phys.* **2012**, *137*, No. 054306.
(34) Krasnikov, S. A.; Preobrajenski, A. B.; Sergeeva, N. N.; Brzhezinskaya, M. M.; Nesterov, M. A.; Cafolla, A. A.; Senge, M. O.; Vinogradov, A. S. Electronic Structure of Ni(II) Porphyrins and Phthalocyanine Studied by Soft X-Ray Absorption Spectroscopy. *Chem. Phys.* **2007**, *332*, 318−324.
(35) Roberts, E. M.; Koski, W. S. Electron Spin Resonance of Copper Phthalocyanine. *J. Am. Chem. Soc.* **1961**, *83*, 1865−1867.
(36) Barraclough, C. G. Diamagnetic Anisotropies of Metal-Free, Nickel(II), and Zinc(II) Phthalocyanines. *J. Chem. Phys.* **1971**, *55*, 1426.
(37) Martin, R. L.; Mitra, S. Paramagnetic Anisotropy and Electronic Structure of $\beta$-Copper(II) Phthalocyanine. *Inorg. Chem.* **1970**, *9*, 182−183.
(38) Mugarza, A.; Robles, R.; Krull, C.; Korytár, R.; Lorente, N.; Gambardella, P. Electronic and Magnetic Properties of Molecule-Metal Interfaces: Transition-Metal Phthalocyanines Adsorbed on Ag(100). *Phys. Rev. B* **2012**, *85*, No. 155437.
(39) Figgis, B. N.; Kucharski, E. S.; Reynolds, P. A. Electronic Structure of Cobalt Phthalocyanine: A Charge Density Study. *J. Am. Chem. Soc.* **1989**, *111*, 1683−1692.
(40) Martin, R. L.; Mitra, S. Paramagnetic Anisotropy and Ground State of $\beta$-Cobalt(II) Phthalocyanine. *Chem. Phys. Lett.* **1969**, *3*, 183−184.
(41) Lever, A. B. P. 336. The Magnetic Behaviour of Transition-Metal Phathalocyanines. *J. Chem. Soc.* **1965**, 1821−1829.
(42) Serri, M.; Wu, W.; Fleet, L. R.; Harrison, N. M.; Hirjibehedin, C. F.; Kay, C. W.; Fisher, A. J.; Aeppli, G.; Heutz, S. High-Temperature Antiferromagnetism in Molecular Semiconductor Thin Films and Nanostructures. *Nat. Commun.* **2014**, *5*, 3079.
(43) Nakamura, K.; Kitaoka, Y.; Akiyama, T.; Ito, T.; Weinert, M.; Freeman, A. J. Constraint Density Functional Calculations for Multiplets in a Ligand-Field Applied to Fe-Phthalocyanine. *Phys. Rev. B* **2012**, *85*, No. 235129.
(44) Evangelisti, M.; Bartolomé, J.; de Jongh, L.; Filoti, G. Magnetic Properties of $\alpha$-Iron(II) Phthalocyanine. *Phys. Rev. B* **2002**, *66*, No. 144410.
(45) Filoti, G.; Kuz'min, M. D.; Bartolomé, J. Mössbauer Study of the Hyperfine Interactions and Spin Dynamics in $\alpha$-Iron(II) Phthalocyanine. *Phys. Rev. B* **2006**, *74*, No. 134420.
(46) Gargiani, P.; et al. Spin and Orbital Configuration of Metal Phthalocyanine Chains Assembled on the Au(110) Surface. *Phys. Rev. B* **2013**, *87*, No. 165407.
(47) Bartolomé, J.; Bartolomé, F.; García, L. M.; Filoti, G.; Gredig, T.; Colesniuc, C. N.; Schuller, I. K.; Cezar, J. C. Highly Unquenched Orbital Moment in Textured Fe-Phthalocyanine Thin Films. *Phys. Rev. B* **2010**, *81*, No. 195405.
(48) Stillman, M. J.; Thomson, A. J. Assignment of the Charge-Transfer Bands in Some Metal Phthalocyanines. Evidence for the S = 1 State of Iron(II) Phthalocyanine in Solution. *J. Chem. Soc., Faraday Trans. 2* **1974**, *70*, 790−804.
(49) Barraclough, C. G. Paramagnetic Anisotropy, Low Temperature Magnetization, and Electronic Structure of Iron(II) Phthalocyanine. *J. Chem. Phys.* **1970**, *53*, 1643.
(50) Thole, B. T.; Van Der Laan, G.; Butler, P. H. Spin-Mixed Ground State of Fe Phthalocyanine and the Temperature-Dependent Branching Ratio in X-ray Absorption Spectroscopy. *Chem. Phys. Lett.* **1988**, *149*, 295−299.
(51) Labarta, A.; Molins, E.; Viñas, X.; Tejada, J.; Caubet, A.; Alvarez, S. Electronic Structure Determination of Iron(II) Phthalocyanine via Magnetic Susceptibility and Mössbauer Measurements. *J. Chem. Phys.* **1984**, *80*, 444.
(52) Gredig, T.; Colesniuc, C. N.; Crooker, S. A.; Schuller, I. K. Substrate-Controlled Ferromagnetism in Iron Phthalocyanine Films Due to One-Dimensional Iron Chains. *Phys. Rev. B* **2012**, *86*, No. 014409.
(53) Gredig, T.; Gentry, K. P.; Colesniuc, C. N.; Schuller, I. K. Control of Magnetic Properties in Metallo-Organic Thin Films. *J. Mater. Sci.* **2010**, *45*, 5032−5035.
(54) Barraclough, C. G. Paramagnetic Anisotropy, Electronic Structure, and Ferromagnetism in Spin S = 3/2 Manganese(II) Phthalocyanine. *J. Chem. Phys.* **1970**, *53*, 1638.
(55) Mitra, S.; Gregson, A. K.; Hatfield, W. E.; Weller, R. R. Single-Crystal Magnetic Study on Ferromagnetic Manganese(II) Phthalocyaninate. *Inorg. Chem.* **1983**, *22*, 1729−1732.
(56) Miyoshi, H.; Ohya-Nishiguchi, H.; Deguchi, Y. The Magnetic Properties of Manganese(II) Phthalocyanine. *Bull. Chem. Soc. Jpn.* **1973**, *46*, 2724−2728.
(57) Petraki, F.; Peisert, H.; Hoffmann, P.; Uihlein, J.; Knupfer, M.; Chassé, T. Modification of the 3d-Electronic Configuration of Manganese Phthalocyanine at the Interface to Gold. *J. Phys. Chem. C* **2012**, *116*, 5121−5127.
(58) Kataoka, T.; et al. Electronic Configuration of Mn Ions in the $\pi$-d Molecular Ferromagnet $\beta$-Mn Phthalocyanine Studied by Soft X-ray


DOI: 10.1021/jp512935v
*J. Phys. Chem. C* 2015, 119, 9805−9815

Magnetic Circular Dichroism. *Solid State Commun.* **2012**, *152*, 806−809.
(59) Williamson, B. E.; VanCott, T. C.; Boyle, M. E.; Misener, G. C.; Stillman, M. J.; Schatz, P. N. Determination of the Ground State of Manganese Phthalocyanine in an Argon Matrix Using Magnetic Circular Dichroism and Absorption Spectroscopy. *J. Am. Chem. Soc.* **1992**, *114*, 2412−2419.
(60) Liao, M.-S.; Watts, J. D.; Huang, M.-J. DFT Study of Unligated and Ligated Manganese II Porphyrins and Phthalocyanines. *Inorg. Chem.* **2005**, *44*, 1941−1949.
(61) Reynolds, P. A.; Figgis, B. N. Metal Phthalocyanine Ground States: Covalence and Ab Initio Calculation of Spin and Charge Densities. *Inorg. Chem.* **1991**, *30*, 2294−2300.
(62) Yamada, H.; Shimada, T.; Koma, A. Preparation and Magnetic Properties of Manganese(II) Phthalocyanine Thin Films. *J. Chem. Phys.* **1998**, *108*, 10256−10261.
(63) Caplins, B. W.; Suich, D. E.; Shearer, A. J.; Harris, C. B. Metal/Phthalocyanine Hybrid Interface States on Ag(111). *J. Phys. Chem. Lett.* **2014**, *5*, 1679−1684.
(64) Kröger, I.; Bayersdorfer, P.; Stadtmüller, B.; Kleimann, C.; Mercurio, G.; Reinert, F.; Kumpf, C. Submonolayer Growth of $H_2$-Phthalocyanine on Ag(111). *Phys. Rev. B* **2012**, *86*, No. 195412.
(65) Nyholm, R.; Mårtensson, N. Experimental Core-Hole Ground State Energies for the Elements $^{41}$Nb to $^{52}$Te. *Solid State Commun.* **1981**, *40*, 311−314.
(66) Leiro, J.; Minni, E.; Suoninen, E. Study of Plasmon Structure in XPS Spectra of Silver and Gold. *J. Phys. F: Met. Phys.* **1983**, *13*, 215.
(67) Bendounan, A.; Cercellier, H.; Fagot-Revurat, Y.; Kierren, B.; Yurov, V.; Malterre, D. Modification of Shockley States Induced by Surface Reconstruction in Epitaxial Ag Films on Cu(111). *Phys. Rev. B* **2003**, *67*, No. 165412.
(68) Wessendorf, M.; Wiemann, C.; Bauer, M.; Aeschlimann, M.; Schneider, M. A.; Brune, H.; Kern, K. Electronic Surface Structure of n-ML Ag/Cu(111) and Cs/n-ML Ag/Cu(111) as Investigated by 2PPE and STS. *Appl. Phys. A: Mater. Sci. Process.* **2004**, *78*, 183−188.
(69) Rojas, G.; Simpson, S.; Chen, X.; Kunkel, D. A.; Nitz, J.; Xiao, J.; Dowben, P. A.; Zurek, E.; Enders, A. Surface State Engineering of Molecule-Molecule Interactions. *Phys. Chem. Chem. Phys.* **2012**, *14*, 4971−4976.
(70) Nakagawa, T.; Takagi, Y.; Matsumoto, Y.; Yokoyama, T. Enhancements of Spin and Orbital Magnetic Moments of Submonolayer Co on Cu(001) Studied by X-ray Magnetic Circular Dichroism Using Superconducting Magnet and Liquid He Cryostat. *Jpn. J. Appl. Phys.* **2008**, *47*, 2132−2136.
(71) Yokoyama, T.; Nakagawa, T.; Takagi, Y. Magnetic Circular Dichroism for Surface and Thin Film Magnetism: Measurement Techniques and Surface Chemical Applications. *Int. Rev. Phys. Chem.* **2008**, *27*, 449−505.
(72) Alfredsson, Y.; et al. Electronic Structure of a Vapor-Deposited Metal-Free Phthalocyanine Thin Film. *J. Chem. Phys.* **2005**, *122*, No. 214723.
(73) Niwa, Y. X-ray Photoelectron Spectroscopy of Tetraphenylporphin and Phthalocyanine. *J. Chem. Phys.* **1974**, *60*, 799.
(74) Alfredsson, Y.; Rensmo, H.; Sandell, A.; Siegbahn, H. Electronic Structure of Thin Film TiOPc Studied by Means of X-ray Absorption and Photoelectron Spectroscopies. *J. Electron Spectrosc. Relat. Phenom.* **2009**, *174*, 50−54.
(75) Calabrese, A.; Floreano, L.; Verdini, A.; Mariani, C.; Betti, M. Filling Empty States in a CuPc Single Layer on the Au(110) Surface Via Electron Injection. *Phys. Rev. B* **2009**, *79*, No. 115446.
(76) Beamson, G.; Moslemzadeh, N.; Weightman, P.; Watts, J. F. Al K$\alpha$ and Cu K$\alpha_1$ Excited XPS of Vanadium Oxide and $VF_3$ Powders: Measurement of the V 1s−KLL Auger Parameters. *J. Electron Spectrosc. Relat. Phenom.* **2008**, *162*, 19−24.
(77) Biesinger, M. C.; Lau, L. W. M.; Gerson, A. R.; Smart, R. S. C. Resolving Surface Chemical States in XPS Analysis of First Row Transition Metals, Oxides and Hydroxides: Sc, Ti, V, Cu and Zn. *Appl. Surf. Sci.* **2010**, *257*, 887−898.
(78) Cui, J.; Da, D.; Jiang, W. Structure Characterization of Vanadium Oxide Thin Films Prepared by Magnetron Sputtering Methods. *Appl. Surf. Sci.* **1998**, *133*, 225−229.
(79) Demeter, M.; Neumann, M.; Reichelt, W. Mixed-Valence Vanadium Oxides Studied by XPS. *Surf. Sci.* **2000**, *454*−*456*, 41−44.
(80) Hryha, E.; Rutqvist, E.; Nyborg, L. Stoichiometric Vanadium Oxides Studied by XPS. *Surf. Interface Anal.* **2012**, *44*, 1022−1025.
(81) Mendialdua, J.; Casanova, R.; Barbaux, Y. XPS Studies of $V_2O_5$, $V_6O_{13}$, $VO_2$ and $V_2O_3$. *J. Electron Spectrosc. Relat. Phenom.* **1995**, *71*, 249−261.
(82) Silversmit, G.; Depla, D.; Poelman, H.; Marin, G. B.; De Gryse, R. Determination of the V2p XPS Binding Energies for Different Vanadium Oxidation States ($V^{5+}$ to $V0^{+}$). *J. Electron Spectrosc. Relat. Phenom.* **2004**, *135*, 167−175.
(83) Werfel, F.; Dräger, G.; Berg, U. X-ray and X-ray Photoelectron Spectra of Vanadium Oxides. *Krist. Tech.* **1981**, *16*, 119−126.
(84) Youn, D.-H.; Kim, H.-T.; Chae, B.-G.; Hwang, Y.-J.; Lee, J.-W.; Maeng, S.-L.; Kang, K.-Y. Phase and Structural Characterization of Vanadium Oxide Films Grown on Amorphous $SiO_2$/Si Substrates. *J. Vac. Sci. Technol., A* **2004**, *22*, 719−724.
(85) Petraki, F.; Peisert, H.; Latteyer, F.; Aygül, U.; Vollmer, A.; Chassé, T. Impact of the 3d Electronic States of Cobalt and Manganese Phthalocyanines on the Electronic Structure at the Interface to Ag(111). *J. Phys. Chem. C* **2011**, *115*, 21334−21340.
(86) Petraki, F.; Peisert, H.; Aygül, U.; Latteyer, F.; Uihlein, J.; Vollmer, A.; Chassé, T. Electronic Structure of FePc and Interface Properties on Ag(111) and Au(100). *J. Phys. Chem. C* **2012**, *116*, 11110−11116.
(87) Hieringer, W.; Flechtner, K.; Kretschmann, A.; Seufert, K.; Auwarter, W.; Barth, J. V.; Gorling, A.; Steinruck, H. P.; Gottfried, J. M. The Surface Trans Effect: Influence of Axial Ligands on the Surface Chemical Bonds of Adsorbed Metalloporphyrins. *J. Am. Chem. Soc.* **2011**, *133*, 6206−6222.
(88) Lukasczyk, T.; Flechtner, K.; Merte, L. R.; Jux, N.; Maier, F.; Gottfried, J. M.; Steinrück, H.-P. Interaction of Cobalt(II) Tetraarylporphyrins with a Ag(111) Surface Studied with Photoelectron Spectroscopy. *J. Phys. Chem. C* **2007**, *111*, 3090−3098.
(89) Petraki, F.; Peisert, H.; Biswas, I.; Chassé, T. Electronic Structure of Co-Phthalocyanine on Gold Investigated by Photoexcited Electron Spectroscopies: Indication of Co Ion−Metal Interaction. *J. Phys. Chem. C* **2010**, *114*, 17638−17643.
(90) Peisert, H.; Kolacyak, D.; Chassé, T. Site-Specific Charge-Transfer Screening at Organic/Metal Interfaces. *J. Phys. Chem. C* **2009**, *113*, 19244−19250.
(91) Ruocco, A.; Evangelista, F.; Gotter, R.; Attili, A.; Stefani, G. Evidence of Charge Transfer at the Cu-Phthalocyanine/Al(100) Interface. *J. Phys. Chem. C* **2008**, *112*, 2016−2025.
(92) Ahmadi, S.; Agnarsson, B.; Bidermane, I.; Wojek, B. M.; Noel, Q.; Sun, C.; Gothelid, M. Site-Dependent Charge Transfer at the Pt(111)-ZnPc Interface and the Effect of Iodine. *J. Chem. Phys.* **2014**, *140*, No. 174702.
(93) Peisert, H.; Petershans, A.; Chasse, T. Charge Transfer and Polarization Screening at Organic/Metal Interfaces: Distinguishing between the First Layer and Thin Films. *J. Phys. Chem. C* **2008**, *112*, 5703−5706.
(94) Baran, J. D.; Larsson, J. A.; Woolley, R. A. J.; Cong, Y.; Moriarty, P. J.; Cafolla, A. A.; Schulte, K.; Dhanak, V. R. Theoretical and Experimental Comparison of SnPc, PbPc, and CoPc Adsorption on Ag(111). *Phys. Rev. B* **2010**, *81*, No. 075413.
(95) Petraki, F.; Peisert, H.; Biswas, I.; Aygül, U.; Latteyer, F.; Vollmer, A.; Chassé, T. Interaction between Cobalt Phthalocyanine and Gold Studied by X-Ray Absorption and Resonant Photoemission Spectroscopy. *J. Phys. Chem. Lett.* **2010**, *1*, 3380−3384.
(96) Stöhr, J. *NEXAFS Spectroscopy*; Springer: Berlin, 2003.
(97) Stöhr, J.; Outka, D. Determination of Molecular Orientations on Surfaces from the Angular Dependence of Near-Edge X-ray-Absorption Fine-Structure Spectra. *Phys. Rev. B* **1987**, *36*, 7891−7905.
(98) Willey, T. M.; Bagge-Hansen, M.; Lee, J. R.; Call, R.; Landt, L.; van Buuren, T.; Colesniuc, C.; Monton, C.; Valmianski, I.; Schuller, I.


DOI: 10.1021/jp512935v
*J. Phys. Chem. C* 2015, 119, 9805−9815

K. Electronic Structure Differences between $H_2$-, Fe-, Co-, and Cu-Phthalocyanine Highly Oriented Thin Films Observed Using NEXAFS Spectroscopy. *J. Chem. Phys.* **2013**, *139*, No. 034701.
(99) Rocco, M. L. M.; Frank, K. H.; Yannoulis, P.; Koch, E. E. Unoccupied Electronic Structure of Phthalocyanine Films. *J. Chem. Phys.* **1990**, *93*, 6859.
(100) Koch, E. E.; Jugnet, Y.; Himpsel, F. J. High-Resolution Soft X-Ray Excitation Spectra of 3d-Metal Phthalocyanines. *Chem. Phys. Lett.* **1985**, *116*, 7−11.
(101) De Francesco, R.; Stener, M.; Fronzoni, G. Theoretical Study of Near-Edge X-Ray Absorption Fine Structure Spectra of Metal Phthalocyanines at C and N K-Edges. *J. Phys. Chem. A* **2012**, *116*, 2885−2894.
(102) Kim, C. M.; DeVries, B. D.; Frühberger, B.; Chen, J. G. A HREELS and NEXAFS Characterization of the Atomic and Molecular Oxygen Species on a Vanadium (110) Surface. *Surf. Sci.* **1995**, *327*, 81−92.
(103) Betti, M. G.; Gargiani, P.; Frisenda, R.; Biagi, R.; Cossaro, A.; Verdini, A.; Floreano, L.; Mariani, C. Localized and Dispersive Electronic States at Ordered FePc and CoPc Chains on Au(110). *J. Phys. Chem. C* **2010**, *114*, 21638−21644.
(104) Sato, M. Electron Spin Resonance Study of Vanadyl Phthalocyanine. *J. Chem. Phys.* **1969**, *50*, 558.
(105) Stepanow, S.; Miedema, P. S.; Mugarza, A.; Ceballos, G.; Moras, P.; Cezar, J. C.; Carbone, C.; de Groot, F. M. F.; Gambardella, P. Mixed-Valence Behavior and Strong Correlation Effects of Metal Phthalocyanines Adsorbed on Metals. *Phys. Rev. B* **2011**, *83*, No. 220401(R).
(106) Chen, X.; Fu, Y.-S.; Ji, S.-H.; Zhang, T.; Cheng, P.; Ma, X.-C.; Zou, X.-L.; Duan, W.-H.; Jia, J.-F.; Xue, Q.-K. Probing Superexchange Interaction in Molecular Magnets by Spin-Flip Spectroscopy and Microscopy. *Phys. Rev. Lett.* **2008**, *101*, No. 197208.
(107) Miyoshi, H. The Magnetic Properties of Manganese(II) Phthalocyanine. II. *Bull. Chem. Soc. Jpn.* **1974**, *47*, 561−565.
(108) Goodenough, J. B. *Magnetism and the Chemical Bond*; Wiley: New York, 1963.
(109) Lee, S.; Yudkowsky, M.; Halperin, W. P.; Ogawa, M. Y.; Hoffman, B. M. One-Dimensional Magnetism in Copper Phthalocyanine. *Phys. Rev. B* **1987**, *35*, 5003−5007.
(110) Javaid, S.; et al. Impact on Interface Spin Polarization of Molecular Bonding to Metallic Surfaces. *Phys. Rev. Lett.* **2010**, *105*, No. 077201.



DOI: 10.1021/jp512935v
*J. Phys. Chem. C* 2015, 119, 9805−9815